AIP Advances

Electrical hysteresis characteristics in photogenerated currents on laser-beam-derived in-plane lateral 1D MoS_2-Schottky junctions

Cite as: AIP Advances **12**, 105210 (2022); https://doi.org/10.1063/5.0098198
Submitted: 06 August 2022 • Accepted: 20 September 2022 • Published Online: 18 October 2022

M. Kosugi, R. Obata, K. Otsuka, et al.

Electrical hysteresis characteristics in photogenerated currents on laser-beam-derived in-plane lateral 1D MoS_2-Schottky junctions

Cite as: AIP Advances 12, 105210 (2022); doi: 10.1063/5.0098198
Submitted: 6 August 2022 • Accepted: 20 September 2022 •
Published Online: 18 October 2022

M. Kosugi,[1] R. Obata,[1] K. Otsuka,[2] K. Kuroyama,[3] S. Du,[3] S. Maruyama,[2] K. Hirakawa,[3] and J. Haruyama[1,3,a)]

AFFILIATIONS

[1] Faculty of Science and Engineering, Aoyama Gakuin University, 5-10-1 Fuchinobe, Sagamihara, Kanagawa 252-5258, Japan
[2] Department of Mechanical Engineering, The University of Tokyo, 7-3-1 Hongo, Bunkyo-ku, Tokyo 113-8656, Japan
[3] Institute for Industrial Sciences, The University of Tokyo, 4-6-1 Komaba, Meguro-ku, Tokyo 153-8505, Japan

[a)] Author to whom correspondence should be addressed: J-haru@ee.aoyama.ac.jp

ABSTRACT

Atomically thin two-dimensional transition-metal dichalcogenide materials with van der Waals integration provide various interesting optoelectronic characteristics that can be used to realize highly efficient flexible solar cells and photosensors. We previously reported in-plane lateral one-dimensional Schottky junctions (SJs) on few-atom-layer 2H-phase semiconductor-molybdenum disulfide by forming a 1T′-metal phase using laser beam (LB) irradiation and clarified their unique optoelectronic properties. Although the LB-derived 1T′/2H phase SJs provided efficient photocurrent generation, they had a large number of defects owing to the excess heat accumulation caused by the LB. Here, we observe partial electric hysteresis properties in photogenerated currents (I_{photo}) on the SJs under reverse bias voltage regions and reveal that they are very sensitive to the voltage sweep direction and its switching (holding) time. The properties persist under dark ambient conditions for a few minutes, even after photo-irradiation is complete. The temperature dependence reveals that a defect-derived deep carrier trap-center, which is unique to the present 1T′ phase, can be the cause of these phenomena. A larger I_{photo} and an increase in photogeneration efficiency are obtained by eliminating this trap center through thermal annealing. In contrast, it is expected that these hysteresis properties lead to atomically thin photo-memristor devices for opto-neuromorphic systems.

The development of flexible and (semi)transparent optoelectronic devices (e.g., solar cells and photosensors) is crucial to resolving problems in next-generation energy systems. It is well known that semiconductor PN junctions and Schottky junctions (SJs), on which a strong electric field concentrates under an applied reverse voltage region, effectively produce excitons and photocurrents, resulting in high-efficiency optoelectronic devices. Among them, van der Waals (vdW)-assembled atomically thin semiconductors [e.g., the two-dimensional (2D) transition-metal dichalcogenide (TMDC) family of semiconductors] are attracting significant attention because they offer optoelectronic devices with significantly beneficial (semi)transparent layers and high mechanical flexibility.

Various optoelectronic characteristics that could be potentially leveraged to develop highly effective photodetectors have been reported in atomically thin TMDC PN junctions or SJs, such as rapid exciton dissociation due to the lack of an extended depletion region[1] and similar ultrafast charge transfer.[2–4] Similar to solar cells, atomically thin TMDC PN junctions have proven to have good power conversion efficiencies (PCE).[5–9] In contrast, atomically thin (or few-layer) TMDC SJ solar cells are still rare.[10]

However, the presence of defects and impurities at the junction interfaces has hindered the realization of high-performing material systems with excellent optoelectronic properties, which depend on characteristics such as the activation energy, carrier capture cross-section, and time constant.[11–15] In particular, gate bias-induced hysteresis and unpredictable threshold voltage remain unresolved issues owing to defect traps at the interface of 2D material systems. The vdW integration of atomically thin layers has resolved this issue as it results in a clean interface at the layer junctions, especially if graphene electrodes[16] and MESFET structures[17] are utilized. Nevertheless, because vdW integration allows for the formation of only 2D vertical PN junctions or SJs, such materials lack in-plane lateral one-dimensional (1D) junctions.

In contrast, our previous electron beam (EB)-derived in-plane lateral 1D SJs (i.e., junctions of the 2H semiconducting/1T metallic phases) formed on few-layer MoS_2 resolved the above issue.[29] However, because EB irradiation is costly and time-consuming, it was not appropriate for industrial application. Moreover, the 1T-phase quickly returns to the 2H-phase (e.g., within 10 days). Thus, we created the 1T′-metallic phase by irradiating a laser beam to the 2H semiconducting phase via in-plane heat, leading to the 1T′/2H-phase in-plane lateral 1D SJs, which is chemically and thermally stable over a long time.[18–24] The SJ realized the highly efficient generation of photocurrents (I_{photo}) under its reverse voltage region, which is widely available for industrial application because of the simple and inexpensive fabrication methods.

However, the transition to the 1T′-phase caused by in-plane heat (e.g., ∼300 °C) degraded the crystal quality and, in some cases, introduced a large number of defects because of the excess heat accumulation.[18] Therefore, an investigation of the defect-related interface quality of the 1T′/2H phase in-plane 1D SJs is indispensable for improving the efficiency of I_{photo} generation as a photosensor. The present observation of electric hysteresis properties under photo-irradiation with different holding times clarifies this via observation of charge trapping and recombination through defect-based energy levels.

In this paper, a 2H-phase n-type semiconducting MoS_2 flake [Fig. 1(a)] is attached to an SiO_2/Si substrate using a mechanical exfoliation method of the bulk material (hq graphene) by Scotch tape and is oxidized by exposure to air for n-type semiconducting properties. The number of layers (∼10) was confirmed by cross-sectional atomic force microscopy and Raman spectroscopy [E_{2g} and A_{1g} peaks in Fig. 1(c)]. An LB (wavelength of ∼532 nm, diameter of ∼1 μm, power of ∼4 mW, and time of ∼10 s per point, which gave the smallest number of defects[18–20]) was irradiated onto the MoS_2 flake and scanned with an ∼0.2 μm overlapping region over an area of ∼8 × 2 μm^2 [as indicated by the red dotted rectangle in Fig. 1(a)], resulting in the creation of the 1T′ phase, following our previous method.[18] The bottom-side 1T′ metallic layers persisted after the LB irradiation from an in-plane lateral 1T′/2H 1D SJ [red arrow in Fig. 1(a)].[25] LB non-irradiated (2H) and irradiated (1T′) regions were confirmed by photoluminescence (PL) and Raman spectroscopy.[26]

The I_{sd}–V_{sd} characteristics [between electrodes A and B in Fig. 1(a)] similar to those in our previous samples[18] are confirmed under dark and light ambient conditions [solid curves in Figs. 1(d) and 1(e)].[27] The I_{sd}–V_{sd} curve shows a weak asymmetric feature in the dark at V_{bg} = −19 V (i.e., a slightly larger I_{sd} in the +V_{sd} region), while I_{sd} drastically increases in the −V_{sd} region under light conditions [Fig. 1(d)]. This suggests the presence of a 1D SJ at the interface between the LB-irradiated and non-irradiated regions (i.e., 1T′ metallic and 2H n-type semiconducting MoS_2 regions, respectively) as mentioned above [see Fig. 4(a)], following our previous reports.[18,28] The photogenerated I_{sd} (I_{photo}) normalized by dark current (I_{eff}) demonstrates a drastic increase of ∼60 times [Fig. 1(e)].[18] The drastic increase in I_{eff} in the −V_{sd} region [Fig. 1(e)] is also in good agreement with our previous results,[18] which revealed an effective generation of excitons by the concentration of high electric fields at the 1D SJ within a reverse-biased voltage region [Fig. 4(b)].[28]

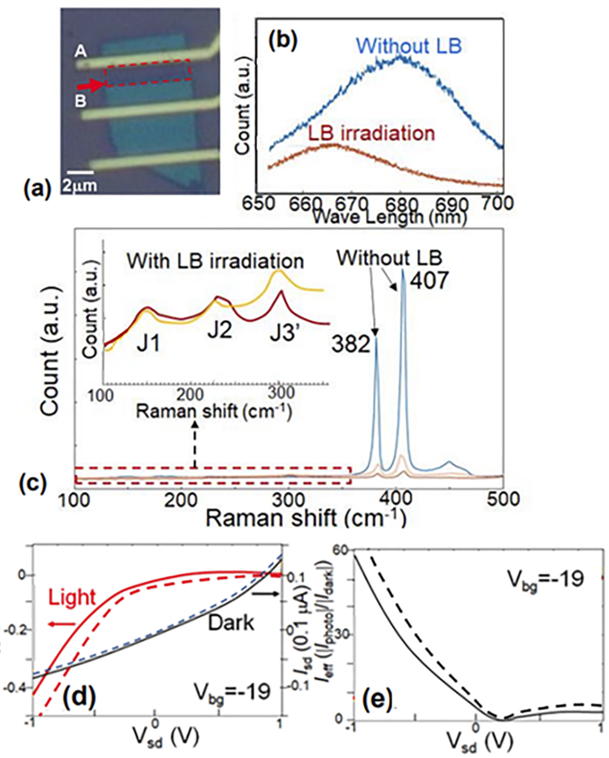

FIG. 1. (a) Optical microscopy image of a few-layer 2H–MoS_2 flake fabricated by mechanical exfoliation of the bulk material with an LB-irradiation region (1T′ region shown in a red dotted rectangle), an in-plane lateral 1D 1T′/2H phase SJ (indicated in a red arrow), and three Au/Ti electrodes. The irradiated regions become semitransparent owing to the reduced thickness.[25] Two electrodes (A and B) are used for all the electrical measurements. (b) PL spectra of the LB-irradiated 1T′ metallic and non-irradiated 2H semiconducting regions. The measured wavelength is 640–700 nm and the size of each rectangle is 1 μm^2. (c) Raman spectra of LB-irradiated and non-irradiated regions in (a). **Inset**: Expansion of the main panel for the 100–350 cm^{-1} region (shown in a dotted rectangle). (d) Source–drain current (I_{sd}) measured between electrodes A and B in Fig. 1(a) under ambient light and dark conditions. Solid and dotted curves correspond to the results before and after the high-vacuum annealing, respectively. All measurements shown here are carried out before the annealing. A solar cell simulator with standard test cell conditions (AM1.5G) was used. (e) Generation efficiency (I_{eff}) of the photocurrent (I_{photo}); I_{photo} normalized by dark currents. Solid and dotted curves indicate the same conditions as those in (d).

Here, we observe small hysteresis properties in the I_{sd}–V_{sd} features (i.e., different I_{sd}–V_{sd} depending on the direction of the applied V_{sd}) at $V_{bg} = -19$ V in the dark [Figs. 2(a) and 2(b)]. I_{sd} is slightly reduced as V_{sd} sweeps from the $-V_{sd}$ to $+V_{sd}$ regions (shown as 2 by an arrow in each figure) after V_{sd} is swept from $+V_{sd}$ to $-V_{sd}$ (shown as 1 by an arrow) [Fig. 2(a)]. However, this property becomes unstable when V_{sd} is swept from $-V_{sd}$ to $+V_{sd}$ and back from $+V_{sd}$ to $-V_{sd}$ [Fig. 2(b)]. These properties are almost independent of the switching time [holding time (t_h), i.e., 30, 60, 90, and 120 s], in which a $\pm V_{sd}$ sweep is stopped and kept at a constant $V_{sd} = \pm 1$ V.

Such partial hysteresis properties become more significant in the reverse V_{sd} regions of the SJ under light irradiation [Figs. 2(c) and 2(d)]. The I_{photo} trends for the V_{sd} sweep direction are qualitatively the same as those in Figs. 2(a) and 2(b). However, a strong t_h dependence is observed in this case. When the voltage is swept from $+V_{sd}$ to $-V_{sd}$ (shown as 1) and kept at a constant $V_{sd} = -1$ V for t_h, the longer t_h (e.g., 120 s; green dotted line) results in a lower $-I_{photo}$ in the V_{sd} sweep from the $-V_{sd}$ to $+V_{sd}$ regions [dotted lines shown as 2 in Fig. 2(c) and the inset]. In contrast, when the voltage is first swept from $-V_{sd}$ (shown as 1) and kept at a constant $V_{sd} = +1$ V, the shorter t_h (e.g., 30 s; red dotted lines) leads to a lower $-I_{photo}$ in the V_{sd} sweep from $-V_{sd}$ to $+V_{sd}$ [dotted lines shown as 2 in Fig. 2(d) and the inset]. These characteristics are more evident in Figs. 2(e) and 2(f) from quantitative viewpoints. Since the application of $V_{sd} > \pm 1$ V electrostatically destroyed the SJs, owing to the concentration of the excess high-electric fields, and resulted in no current flow in the devices, V_{sd} was applied within $V_{sd} = \pm 1$ V for the present measurements.

Moreover, it is revealed that such partial hysteresis properties with reduced I_{sd} qualitatively persist even under dark ambient conditions for at least $t = 6$ min after the above-mentioned Fig. 2 measurements under light conditions are completed, as shown in Fig. 3(a) and the inset. Figure 3(b) shows the changes in the ratio of I_{sd} corresponding to Fig. 3(a) (i.e., the I_{sd} values of solid lines/dotted lines), depending on time (t) after the above-mentioned Fig. 2 measurements are completed. The ratio decreases to half its value after $t = 2$ min has passed (i.e., from a ratio of 4 at $t = 0$–2 at $t = 2$) and reduces further below 1 after $t = 4$ min. However, it should be noted that the ratio of 2 persisted in the dark for 2 min, even after the measurements under ambient light conditions were completed.

We qualitatively discuss the observed hysteresis properties. The observed hysteresis properties in the I_{sd}–V_{sd} features conventionally suggest the presence of defects, which act as trap centers for photogenerated electrons or holes, at the (1D lateral) SJ interfaces.

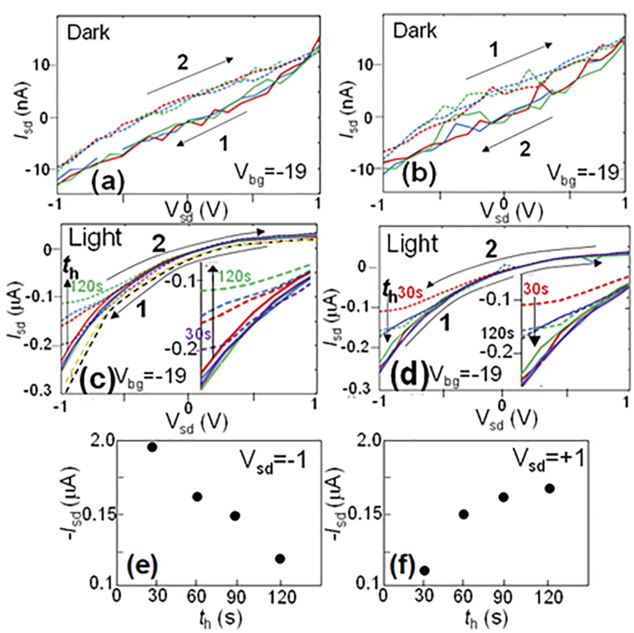

FIG. 2. (Partial) hysteresis properties in the I_{sd}–V_{sd} plots at $V_{bg} = -19$ V in the dark [(a) and (b)] and under ambient light [(c) and (d)] conditions. The arrows indicate the V_{sd} sweep directions. For (a) and (c), a constant $V_{sd} = -1$ V is kept for t_h (30, 60, 90, 120 s) after the voltage is swept from $+V_{sd}$ to $-V_{sd}$ (shown as 1; solid lines) and, then, the voltage is swept back from $-V_{sd}$ to $+V_{sd}$ [shown as 2; dotted lines; 30 s (black), 60 s (red), 90 s (blue), 120 s (green)]. For (b) and (d), a constant $V_{sd} = +1$ V is kept for t_h (30, 60, 90, 120 s) after the voltage is swept from $-V_{sd}$ to $+V_{sd}$ (shown as 1; solid lines) and, then, the voltage is swept back from $+V_{sd}$ to $-V_{sd}$ [shown as 2; dotted lines; 30 s (red), 60 s (blue), 90 s (green), 120 s (black)]. Black (swept from $+V_{sd}$ to $-V_{sd}$) and yellow (from $-V_{sd}$ to $+V_{sd}$) dotted curves with $t_h = 120$ s indicate the results after the high-vacuum annealing. **Insets of** (c) and (d): Expansion of each main panel around the hysteresis curves ($V_{sd} < \sim -0.5$ V). (e) and (f) $-I_{sd}$ values as a function of t_h corresponding to the dotted color lines in (c) and (d).

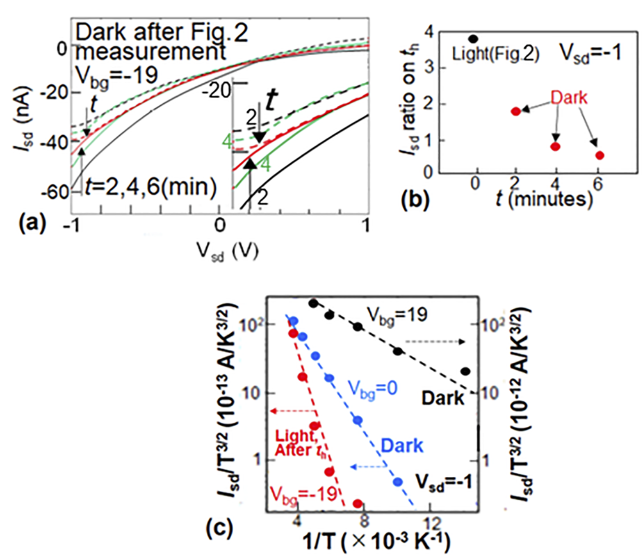

FIG. 3. (a) Partial hysteresis properties under dark ambient conditions, which are the same as those in Fig. 2(c) ($t_h = 120$ s), observed after the measurements under ambient light conditions (Fig. 2) have been completed, depending on time [t minutes; line colors in black (2 min), green (4 min), and red (6 min)]. **Inset**: Expansion of the main panel around the hysteresis curves ($V_{sd} < \sim -0.5$ V). (b) Changes in the ratio of I_{sd} corresponding to (a) (i.e., the ratios of solid lines/dotted line values at $V_{sd} = -1$ V for each t; $t = 0$ corresponding to Fig. 2). (c) Arrhenius plot of the normalized conductance vs temperature relationship at two different V_{bg} values, measured under dark ambient conditions following the formalisms for the reverse voltage (i.e., $-V_{sd}$) region of a 2D Schottky model [Eqs. (1)–(3)]. Only the values represented by the red symbols are measured under light after performing the measurements in Fig. 2(c) (i.e., $t_h = 120$ s).

When photo-irradiation is carried out to the lateral SJ under high electric fields caused by reverse V_{sd}, photogenerated electrons and holes flow into the 2H semiconducting and 1T′ metallic regions, respectively, resulting in a drastic increase in I_{photo} [Fig. 4(b)]. However, a reduction in I_{photo} can be caused when excess electrons are trapped by many defects in the 2H region or when excess holes are trapped by many defects in the 1T′ region close to the SJ interface by applying a constant V_{sd} for t_h because sufficient charge trapping relaxes the band difference and concentration of the electric fields [Fig. 4(c)]. This is in good agreement with the I_{photo} reduction in the V_{sd} sweeping to the $+V_{sd}$ region after a longer t_h at $V_{sd} = -1$ V.

In the present structure, the 1T′ metallic area is formed by heat accumulation due to LB irradiation, whereas the 2H semiconducting area is unaffected by the LB. Hence, almost all defects should exist only in the 1T′ region close to the SJ, and holes should be trapped by many defects in the 1T′ region [Fig. 4(c)]. Indeed, the onset of the forward-voltage current is more gradual than that in the EB-derived SJ with fewer defects and free Fermi-level (E_F) pinning, and the estimated ideality factor $\eta \sim 1.2$ (meaning the generation/recombination currents by defects at the SJ) is larger than that in the EB-derived case ($\eta \sim 1.07$) when the forward-voltage current is fitted by the formalism of the 2D SJ. The excess heat accumulation that causes the 1T′ phase may yield a larger concentration of defect centers compared with the EB-derived SJ case.

On the other hand, the V_{sd} sweeping from the $+V_{sd}$ to $-V_{sd}$ regions after the shorter t_h at $V_{sd} = +1$ V leads to a decrease in I_{photo}, and the longer t_h results in a larger I_{photo}. This is because the trapped holes recombine with electrons during t_h at a constant $V_{sd} = +1$ V under ambient light conditions [Fig. 4(d)]. The shorter t_h at $+V_{sd}$ is not sufficient for this recombination, and the captured holes persist, thereby reducing I_{photo}.

Under dark ambient conditions, such carrier trapping and recombination processes are caused only by the application of V_{sd}. Thus, I_{sd} decreases as V_{sd} is swept from the $-V_{sd}$ to $+V_{sd}$ regions after it is swept from $+V_{sd}$ to $-V_{sd}$, resulting in very small hysteresis-like loops [Fig. 2(a)]. These loops become unstable as V_{sd} is swept from $+V_{sd}$ to $-V_{sd}$ after being swept from $-V_{sd}$ to $+V_{sd}$ [Fig. 2(b)]. The independence of t_h under this dark condition suggests that the photo-active carrier trap centers yield the above-mentioned large partial hysteresis properties under ambient light conditions. Nevertheless, the partial hysteresis properties of the reduced I_{sd} persisted even in the dark for a few minutes after Fig. 2 measurements were completed under ambient light conditions [Fig. 3(a)]. This suggests the presence of residual carriers in the defect centers, which may have strong carrier capturing and maintaining characteristics.

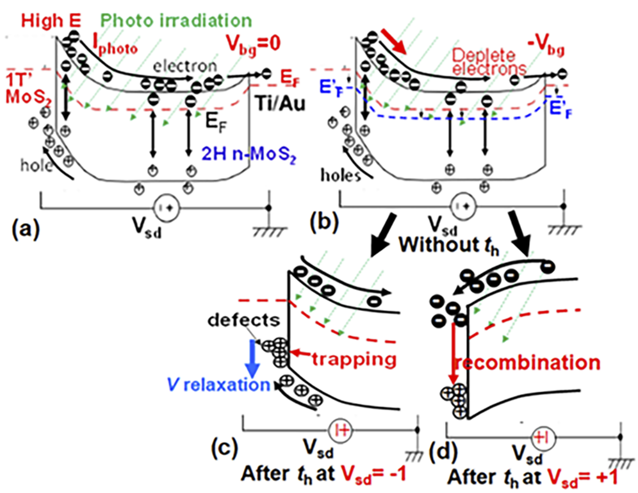

FIG. 4. Schematic views of the energy band diagrams of the SJ for the reverse SJ region (i.e., $-V_{sd}$) at (a) $V_{bg} = 0$ V, (b) $-V_{bg}$, and [(c) and (d)] for Figs. 2(c) and 2(d) experiments.

To confirm this interpretation, the temperature dependence of I_{sd} is measured. Figure 3(c), an Arrhenius plot of the normalized conductance vs temperature relationship, shows the measurements obtained in the dark following the formalisms for the reverse voltage (i.e., $-V_{sd}$) region of a two-dimensional (2D) Schottky model, which are as follows:[3]

$$I_{2D} = WA^*{}_{2D}T^{3/2}\,\exp\left(-\frac{q\emptyset_B}{k_BT}\right), \tag{1}$$

$$A^*{}_{2D} = q\sqrt{8\pi k_B{}^2 m^*/h^2}, \tag{2}$$

$$m^* = 0.45m_0, \tag{3}$$

where ϕ_B is the SJ barrier height, $A^*{}_{2D}$ is the 2D Richardson constant, W is the junction length (~8 μm), k_B is the Boltzmann constant, m^* is the effective mass of MoS_2, and m_0 is the electron mass. All dependencies for two different V_{bg} values show linear relationships with slope values of ~0.14 and ~0.04 eV for V_{bg} values of 0 and 19 V, respectively. The slope values for V_{bg} of 0 and +19 V are almost the same as those for ϕ_B reported in our previous experiments using similar samples with the 1T′/2H SJs, implying that they can correspond to ϕ_B, which suggests the presence of 1D lateral SJs.

However, no such distinct relationships are confirmed at V_{bg} of −19 V under dark ambient conditions. Thus, the same temperature dependence measurement is performed after applying t_h at a constant $V_{sd} = -1$ V under ambient light conditions [i.e., Fig. 2(c) experiment]. This measurement is similar to photoinduced current spectroscopy (PICTS) measurements.[23] A linear relationship with a much larger slope value of ~0.28 eV is reconfirmed, as shown by the red symbols in Fig. 3(c). This result suggests that the reduction in I_{photo} after t_h in Fig. 2(c) can be attributed to the hole capture and accumulation caused by this deep trap center, as shown in Fig. 4(c). Indeed, this relationship becomes ambiguous and almost disappears by the measurement of Fig. 2(d) (i.e., after applying t_h at a constant $V_{sd} = +1$ V under light). These results qualitatively support the strong correlation between the observed hysteresis properties and hole capture and recombination via the deep trap center (~0.28 eV), as shown in Figs. 4(c) and 4(d).

This in-plane 1D SJ provides rapid dissociation of the photogenerated excitons owing to the concentration of high electric fields under the reverse voltage regime. However, the deep trap center in the 1T′ region close to the SJs can capture photogenerated holes rapidly before they diffuse into the electrodes. Moreover, because this trap center is quite deep, it can tightly maintain carriers (i.e., memory effect) for a few minutes even after photo-irradiation is stopped [Fig. 3(a)]. Because such a photosensitive deep trap center has not been reported in MoS_2, it is unique to the present 1T′ phase yielded by the LB-derived excess heat.

The observed partial hysteresis properties in I_{photo} can be eliminated by thermal annealing of the samples (at ~350 °C under a high vacuum of ~10^{-6} Torr for 30 min), resulting in the increase in I_{photo} and I_{eff} [dotted curves in Figs. 1(d) and 1(e); black and yellow dotted curves in Fig. 2(d)], which is four times higher than that in our previous report. This realizes higher-efficiency photo-sensors. In contrast, these hysteresis properties, which are caused by the photo- and V_{sd}-sensitive deep trap center, can open a door to create atomically thin opto-neuromorphic devices, such as SJ photo-memristors, in which the application of a pulsed $\pm V_{sd}$ to the 1D SJs leads to the realization of consistent bipolar and analog switching exhibiting synapse-like learning behavior, controlled by photo-irradiation.[24]

The authors thank J. Oka, S. Noda, S. Murakami, T. Yamamoto, S. Tarucha, Y. Shiomi, E. Saito, T. Ando, and T. Enoki for their technical contributions, fruitful discussions, and encouragement. The work performed at Aoyama Gakuin University was supported by the Aoyama Gakuin University Research Institute grant program for the creation of innovative research. The section of work performed at the University of Tokyo was also supported by JSPS KAKENHI (Grant Nos. JP20H05660, JP19J01737, and JP20K14384 for K.K. and K.H., and Grant No. JP20H00220 for S.M.), and by JST, CREST under Grant No. JPMJCR20B5, Japan for S.M.

AUTHOR DECLARATIONS

Conflict of Interest

The authors have no conflicts to disclose.

Author Contributions

M. Kosugi: Data curation (equal); Investigation (equal). **R. Obata**: Data curation (equal); Investigation (equal). **K. Otsuka**: Supervision (equal). **K. Kuroyama**: Supervision (equal). **S. Du**: Supervision (equal). **S. Maruyama**: Supervision (equal). **K. Hirakawa**: Supervision (equal). **J. Haruyama**: Project administration (equal); Supervision (equal); Writing – original draft (equal).

DATA AVAILABILITY

The data that support the findings of this study are available within the article.

REFERENCES

[1] C.-H. Lee, G.-H. Lee, A. M. van der Zande, W. Chen, Y. Li, M. Han, X. Cui, G. Arefe, C. Nuckolls, T. F. Heinz, J. Guo *et al.*, Nat. Nanotechnol. **9**, 676 (2014).

[2] X. Hong, J. Kim, S.-F. Shi, Y. Zhang, C. Jin, Y. Sun, S. Tongay, J. Wu, Y. Zhang, and F. Wang, Nat. Nanotechnol. **9**, 682 (2014).

[3] Y. Katagiri, T. Nakamura, A. Ishii, C. Ohata, M. Hasegawa, S. Katsumoto, T. Cusati, A. Fortunelli, G. Iannaccone, G. Fiori, S. Roche, and J. Haruyama, Nano Lett. **16**, 3788 (2016).

[4] Y. Katagiri, T. Nakamura, S. Katsumoto, and J. Haruyama, Appl. Phys. Lett. **110**, 143109 (2017).

[5] O. Lopez-Sanchez, E. Alarcon Llado, V. Koman, A. Fontcuberta i Morral, A. Radenovic, and A. Kis, ACS Nano **8**, 3042 (2014).

[6] M.-L. Tsai, S.-H. Su, J.-K. Chang, D.-S. Tsai, C.-H. Chen, C.-I. Wu, L.-J. Li, L.-J. Chen, and J.-H. He, ACS Nano **8**, 8317 (2014).

[7] S. Memaran, N. R. Pradhan, Z. Lu, D. Rhodes, J. Ludwig, Q. Zhou, O. Ogunsolu, P. M. Ajayan, D. Smirnov, A. I. Fernández-Domínguez *et al.*, Nano Lett. **15**, 7532 (2015).

[8] B. W. H. Baugher, H. O. H. Churchill, Y. Yang, and P. Jarillo-Herrero, Nat. Nanotechnol. **9**, 262 (2014).

[9] R. Cheng, D. Li, H. Zhou, C. Wang, A. Yin, S. Jiang, Y. Liu, Y. Chen, Y. Huang, and X. Duan, Nano Lett. **14**, 5590 (2014).

[10] T. Akama, W. Okita, R. Nagai, C. Li, T. Kaneko, and T. Kato, Sci. Rep. **7**, 11967 (2017).

[11] A. Y. Polyakov, N. B. Smirnov, A. V. Govorkov, A. V. Markov, A. M. Dabiran, A. M. Wowchak, A. V. Osinsky, B. Cui, P. P. Chow, S. J. Pearton, and S. J. Pearton, Appl. Phys. Lett. **91**, 232116 (2007).

[12] T. Fujii, M. Kawasaki, A. Sawa, H. Akoh, Y. Kawazoe, Y. Tokura, Appl. Phys. Lett. **86**, 012107 (2005).

[13] K. Choi, S. R. A. Raza, H. S. Lee, P. J. Jeon, A. Pezeshki, S.-W. Min, J. S. Kim, W. Yoon, S.-Y. Ju, K. Lee, and S. Im, Nanoscale **7**, 5617 (2015).

[14] H. Kwon, P. J. Jeon, J. S. Kim, T.-Y. Kim, H. Yun, S. W. Lee, T. Lee, and S. Im, 2D Mater. **3**, 044001 (2016).

[15] X. Zou, J. Wang, C.-H. Chiu, Y. Wu, X. Xiao, C. Jiang, W.-W. Wu, L. Mai, T. Chen, J. Li *et al.*, Adv. Mater. **26**, 6255 (2014).

[16] H. G. Shin *et al.*, Nano Lett. **18**, 1937 (2018).

[17] H. S. Lee, S. S. Baik, K. Lee, S.-W. Min, P. J. Jeon, J. S. Kim, K. Choi, H. J. Choi, J. H. Kim, and S. Im, ACS Nano **9**, 8312 (2015).

[18] Y. Nagamine, J. Sato, Y. Qian, T. Inoue, T. Nakamura, S. Maruyama, S. Katsumoto, and J. Haruyama, Appl. Phys. Lett. **117**, 043101 (2020).

[19] H. Mine, A. Kobayashi, T. Nakamura, T. Inoue, S. Pakdel, D. Marian, E. Gonzalez-Marin, S. Maruyama, S. Katsumoto, A. Palacios, and J. Haruyama *et al.*, Phys. Rev. Lett. **123**, 146803 (2019).

[20] N. Katsuragawa, T. Nakamura, T. Inoue, S. Pakdel, S. Maruyama, S. Katsumoto, J. J. Palacios, and J. Haruyama, Commun. Mater. **1**, 51 (2020).

[21] S. Cho, S. Kim, J. H. Kim, J. Zhao, J. Seok, D. H. Keum, J. Baik, D.-H. Choe, K. J. Chang, K. Suenaga *et al.*, Science **349**, 625 (2015).

[22] S. Tang, C. Zhang, D. Wong, Z. Pedramrazi, H.-Z. Tsai, C. Jia, B. Moritz, M. Claassen, H. Ryu, S. Kahn *et al.*, Nat. Phys. **13**, 683 (2017).

[23] A. Y. Polyakov, N. B. Smirnov, A. V. Govorkov, A. V. Markov, T. G. Yugova, E. A. Petrova, A. M. Dabiran, A. M. Wowchak, A. V. Osinsky, P. P. Chow, S. J. Pearton, K. D. Shcherbatchev, and V. T. Bublik, J. Electrochem. Soc. **154**, H749 (2007).

[24] R. Xu, H. Jang, M.-H. Lee, D. Amanov, Y. Cho, H. Kim, S. Park, H.-j. Shin, and D. Ham, Nano Lett. **19**, 2411 (2019).

[25] LB-generated heat accumulates over the regions scanned by the LB, and the temperature of the regions reaches ~300 °C, resulting in a phase transition from 2H to 1T′ starting from the top surface layer. Because excess heat accumulates from the top surface, such layers burn out and become thinner, resulting in a change to a (semi)transparent appearance [Fig. 1(a)].

[26] The PL signals demonstrate large and small peaks at high and low wavenumbers for the LB non-irradiated (2H) and irradiated (1T′) regions, respectively [Fig. 1(b)]. The former corresponds to the small band gap energy of bulk MoS_2, while the latter could be taken to mean that three layers of bottom-side MoS_2 remained after the top-surface side burned out, and the remaining few-layers transited to the 1T′ metallic phase. The presence of the 1T′ metallic phase was confirmed by Raman spectroscopy [peaks J_1–J_3 in the inset of Fig. 1(c)].[3,18]

[27] Two electrodes [indicated by A and B in Fig. 1(a)] consisting of Ti/Au (20/500 nm), one of which is located in the 1T′ metal region (i.e., LB-irradiated region), while the other is in the 2H region, were formed on both sides of the junction for photocurrent measurements. A back-gate electrode was attached to the back side of the Si substrate with a thick SiO_2 layer (~300 nm).

[28] Because the application of $-V_{bg}$ depletes electrons in the n-type semiconducting region, I_{eff} is significantly induced. In contrast, because electrons are heavily

doped into the n-type semiconducting region by applying $+V_{bg}$ in Fig. 2(d), and the doped electrons significantly contribute to the detected currents, the current increase in $-V_{sd}$ disappears.

[29]Fermi-level (E_F) pinning free from defects and impurities was demonstrated due to the concentration of excess electrical fields at the in-plane 1D SJ.[3,4] In the EB-derived SJ, the 1T metallic phase was imprinted into few-layer 2H-semiconducting MoS_2 by EB irradiation, resulting in the formation of in-plane lateral 1T/2H phase 1D SJs with a barrier height (ϕ_B) in the range of 0.13–0.18 eV.[3] The EB-derived 1T phase crystal had fewer defects because EB irradiation caused less damage, resulting in a small number of defects at the SJ.